Tellus (1999), 51A, 526–549
Printed in UK – all rights reserved

TELLUS
ISSN 0280–6495

Sensitivity of atmosphere–ocean heat exchange and heat content in the North Sea and the Baltic Sea

By CORINNA SCHRUM* and JAN O. BACKHAUS, *Zentrum für Meeres- und Klimaforschung, Universität Hamburg, Troplowitzstr. 7, 22529 Hamburg, Germany*

(Manuscript received 18 September 1997; in final form 5 March 1999)

ABSTRACT

A 3-d baroclinic coupled ice–ocean model, applied to the connected marginal seas, North Sea and Baltic Sea, was used to investigate the seasonal cycle of both heat content of the water column and atmosphere–ocean heat exchange throughout the seasonal cycle. Case studies were carried out to investigate, quantify and inter-compare the intra-annual sensitivity of the thermal state of both marginal seas in response to changes in wind forcing, air temperature and fresh water runoff. The prescribed changes in model forcing were well within the range of the observed variability. A simulation for a representative reference case (1984–84) served to quantify predicted anomalies. Reducing the fresh water runoff for both seas by 30% resulted in a surprisingly small response in the heat content which was one order of magnitude smaller as compared to the applied change in wind forcing. A reduction of the air temperature by 2°C caused a decrease of the heat content throughout the seasonal cycle in the order of 30%. In contrast to a change in air temperature a reduction of 30% in wind stress yielded distinct seasonal differences in the oceanic response. The most significant wind induced changes occurred during autumn and winter in the Baltic Sea and in the North Sea. A reduced wind forcing led to a larger oceanic heat content in winter as a consequence of a reduced winter convection and an intensification of the winter thermocline in the freshwater dominated Baltic. In the Baltic Proper, with its perennial thermo-haline stratification, predicted temperature changes of intermediate waters were several times higher than sea surface temperature changes. Compared with the North Sea, the Baltic showed a much higher sensitivity in response of the heat content to changes in the wind forcing. However, the opposite is true for the heat flux from the water to the atmosphere during the cooling period. Here the sensitivity of the North Sea is much higher than that of the Baltic Sea. This is caused by the fact that advective heat flux changes and atmospheric heat flux changes are working in the same direction in the Baltic Sea and acting in opposite direction in the North Sea. Results of this sensitivity study suggest that future studies on an inter-annual sensitivity should be conducted with a coupled atmosphere–ocean model.

1. Introduction

Natural climate variability and anthropogenic climate change have been under investigation for more than two decades. During recent years, global climate models have been improved and process studies about climate variability and the sensitivity of the climate system have been carried out for atmosphere and ocean (Cubasch et al., 1992, 1995; Roeckner et al., 1992; Johns et al., 1997). However, the horizontal resolution of global climate models is still in the order of hundreds of kilometer, and thus they are not able to give detailed information on a regional scale (a brief discussion was earlier given by Von Storch, 1994). Therefore, downscaling techniques are needed to conclude from the global scale dynamics to the regional scale. This is done in

* Corresponding author.

principle in two different ways, statistical and dynamical downscaling. Using statistical downscaling it is possible to show correlations between large scale signals and regional scale physics (Heyen et al., 1996). However, detailed explanations for the observed correlations cannot be deduced. To get more insight into the processes involved, regional climate models (i.e., dynamical downscaling) are useful tools. For the North Sea and the Baltic Sea (Fig. 1), such a model has been developed and validated (Schrum, 1997a). It was used here to evaluate systematically the influence of air temperature, wind speed and fresh water runoff on thermodynamics, heat budget and ice development during one seasonal cycle. A year (from May 1983 to April 1984) which is in many aspects (fresh water runoff (Bergström and Carlsson, 1994), heat content (Pohlmann, 1996b), sea ice distribution (Haapala et al., 1993) close to the mean state, was chosen to evaluate the thermodynamic sensitivity of both marginal seas, Baltic Sea and North Sea. First, a reference case was calculated by using the original forcing database. As a second step, a sensitivity analysis was performed with respect to changes in air temperature, wind speed and fresh water runoff.

2. Model description

The model is a coupled ice–ocean model. It was applied to the North Sea and the Baltic Sea with

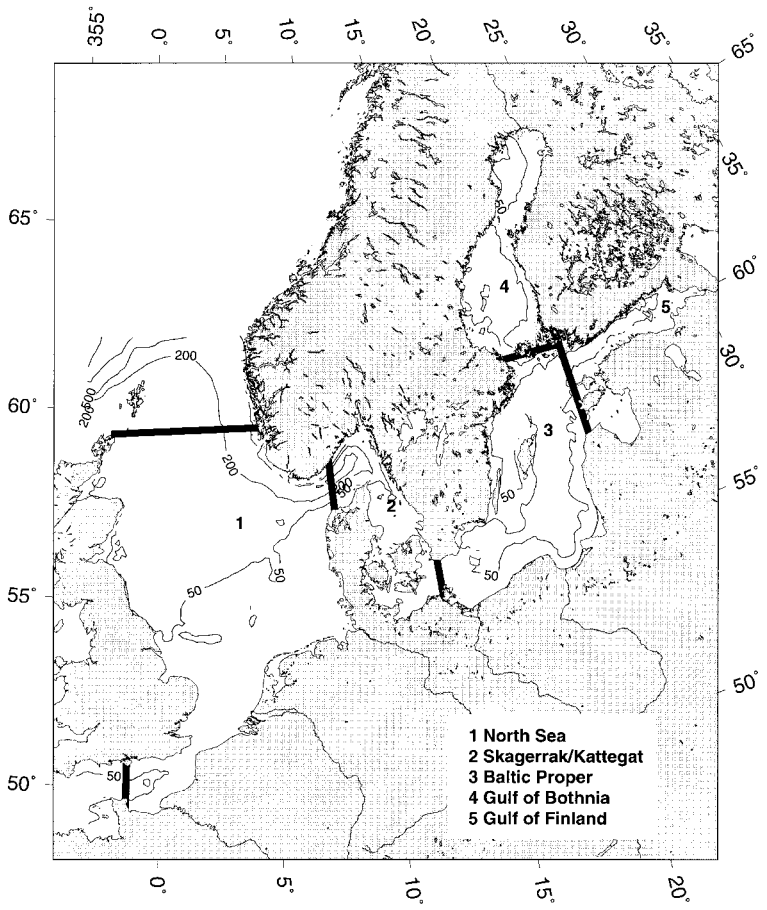

Fig. 1. The region of the North Sea and the Baltic Sea including topographic information. The boundaries of the model and the boundaries of the sub-basins used in the analysis are marked.

a horizontal resolution of 6 nm and a vertical grid spacing which is able to resolve stratification. Twenty layers are used at maximum. For the upper 40 m a vertical resolution of 5 m was used and between 40 and 88 m the vertical grid spacing is 8 m. The lower layers are resolved with coarser resolution, their lower boundaries are at 100, 125, 150, 200, 400 and 630 m depth. The calculated model variables are the 3-d transport field, temperature, salinity, density, sea surface elevation, vertical eddy viscosity and diffusivity, ice compactness, ice thickness, ice velocities and thickness of ridged ice.

The hydrodynamic part of the model is based on the HAMSOM (HAMburg Shelf Ocean Model), which has successfully been applied to several shelf sea regions to investigate hydro- and thermodynamics (Backhaus, 1985; Backhaus and Hainbucher, 1987; Stronach et al., 1993; Daji, 1995; Pohlmann, 1996a; Schrum, 1997b). The HAMSOM is a non-linear primitive equation model. The model equations are given in Section 9. Turbulent vertical exchange processes are calculated with an algebraic first-order k–ε model, in detail described by Pohlmann (1996a), and modified as described by Schrum (1997b), the basics of the turbulence closure are given in Section 10. In the case of unstable stratification a mass conserving convective mixing between the unstable layers is carried out. At the open boundaries daily means of sea surface elevation, temperature and salinity, calculated with a coarser North Sea model (Pohlmann, 1996a) are prescribed. Additionally, a sea surface elevation caused by a M2-tidal forcing is prescribed.

The ice model is a Hibler-type sea–ice model (Hibler, 1979). The dynamic part was first applied to the Baltic Sea by Leppäranta (1981) and completed by a viscous-plastic rheology by Leppäranta and Zhang (1992, unpublished internal report of the Finnish Institute of Marine Research). The model equations are given in Section 11. For this application, the Leppäranta–Zhang-model was completed by a thermodynamic ice model. Both sub-models are thermodynamically and dynamically coupled by the fluxes of momentum, heat and salt, which were calculated from data of air temperature, relative humidity, wind speed and direction and cloudiness by using standard bulk formulae. The basics of the thermodynamics and the model coupling are given in Section 12. The bulk formulae which were used in this application for sensible and latent heat flux are the formulae given by Kondo (1975). Net long-wave radiation was calculated with the Boltzmann radiation law, considering an emissivity of the atmosphere depending only on cloudiness (Maykut, 1986). The global radiation was calculated with a simple radiation model after Dobson and Smith (1988). Wind stress was calculated after a bulk formula given by Luthard (1987). In Section 13, the bulk formulae are given.

In a previous paper (Schrum, 1997a), model configuration and forcing database (for the North Sea: observations, compiled by the Deutschen Wetterdienst, Seewetteramt Hamburg; for the Baltic Sea: the Baltic Sea ice climate dataset (Haapala et al., 1996)) were described in detail and an extended validation of model results with observed sea surface temperature, sea ice conditions and climatological haline and thermal stratification was carried out. It was shown that the model was able to describe realistically the regional and seasonal dynamic and thermodynamic variability during the period May 1983 to April 1984 in both marginal seas.

3. Hydro- and thermodynamics in North Sea and Baltic Sea

The North Sea and Baltic Sea are both fresh water influenced marginal seas. The North Sea receives a direct fresh water inflow by river runoff and by a net surplus of precipitation in the order of 400 km^3/yr (Damm, 1997). The fresh water inflow to the Baltic Sea runs up to a value of 530 km^3/yr. This consists of a river runoff of 480 km^3/yr after Bergström and Carlsson (1994) and a net fresh water input from precipitation minus evaporation of 50 km^3/yr, based on investigations for the period 1951–1970 (HELCOM, 1986) and recent estimates for 1981–1994 from Omstedt et al. (1997), both compared by Omstedt et al. (1997). The fresh water inflow to the Baltic Sea is completely released to the North Sea, in addition to its direct fresh water inflow. However, compared to the Baltic Sea the North Sea is considerably saltier (see predicted mean surface salinity for August 1983, Fig. 2). Mean salinities in the North Sea are around 34 PSU, due to the exchange of the North Sea with the Atlantic

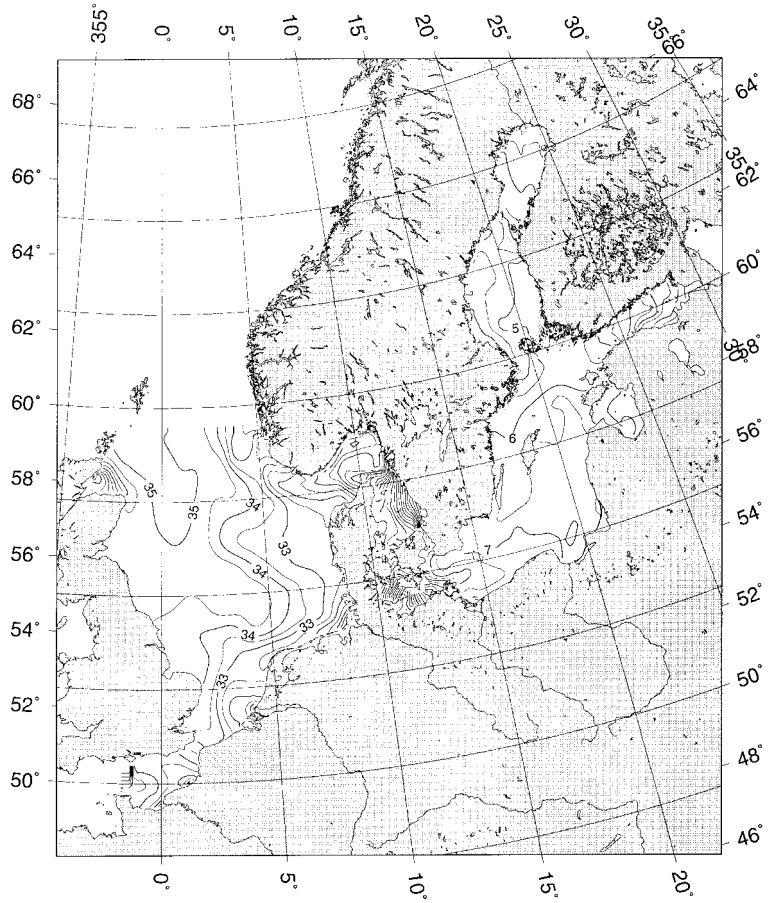

Fig. 2. Calculated monthly mean sea surface salinity (PSU) for August 1983.

Ocean, which can easily take place via the widely open northern boundary. In contrast, the inflow of salty Atlantic and North Sea water into the Baltic Sea is largely hindered by the complex topography in the transition area between the North Sea and the Baltic Sea, and thus, the salinity in the upper and central parts of the water column in the Baltic Sea is well below 8 PSU for most of the Baltic Sea area. Only near the bottom, more saline water, advected from the North Sea to the Baltic Sea, can be found. Studies on the water budget and water exchange of the Baltic Sea were made by several authors (HELCOM, 1986; Stigebrand, 1983). However, the processes were not completely understood and are still under investigation for example in the context of the BALTEX (The Baltic Sea Experiment, International BALTEX Secretariat, 1995) program. An important role for the renewal of Baltic Sea deep water have the wind driven major inflows of salty and thus heavier North Sea water. Matthäus (1995) gave a detailed review on the variability of these sporadic events during the period from 1880 to 1994. He found that most of these events took place in clusters which lasted not more than 5 years.

The thermodynamic behaviour, especially during the winter season, is very different for the North Sea and the Baltic Sea, as earlier explained by Backhaus (1996). This is caused on the one hand by the behaviour of the density of sea water and on the other hand by the existence of the permanent halocline in the Baltic Sea. Because of the relevance for the following investigations, this

will be shortly explained: The temperature of the density maxium is below the freezing point for the North Sea and above the freezing point for the Baltic Sea. This difference is caused by the different salinity characteristic in both basins. Thus, except the small region of the Norwegian Coastal Current, where haline stratification is manifest and stablizes the water column vertically, the North Sea is totally mixed by convection during the winter and the heat reservoir of the North Sea is released unhindered to the atmosphere until the end of the cooling period. In contrast, the convection in the Baltic Sea is restricted to water depths above the halocline due to the strong haline stratification and the thermal energy of waters below the halocline is not available for release to the atmosphere. Furthermore, after the convection period in autumn, when the surface temperature falls below the temperature of the density maxium (in the Baltic between 2 and 4°C), a winter thermocline develops and again hinders the heat exchange between the surface layer and the deeper water. Compared to the North Sea, the thin surface layer is cooled down much faster and favours development of sea ice, which occurs with a high probability in the northern part of the Baltic Sea every year. In regions where a closed ice sheet has developed, the heat exchange between atmosphere and ocean is reduced even more. In Fig. 3, calculated sea surface temperatures and ice conditions for the North Sea and the Baltic Sea are shown. Differences of more than 4°C between the sea surface temperature in the North Sea and the Baltic Proper were calculated.

3.1. *Heat budget*

The seasonal development of the heat budget of the North Sea and the Baltic Sea is discussed by investigations of model results for the reference run for the period from May 83 to April 84. During spring and summer a positive net heat flux into the ocean occurs and the oceanic heat content increases. This surplus is slowly released to the atmosphere during autumn and winter. The calculated heat content in the different sub-basins (the boundaries of the sub-basins are given in Fig. 1) of the North Sea and the Baltic Sea (Fig. 4a) show this seasonal cycle, respectively. However, there are large differences between the magnitude of the total heat content and its cycle for the sub-basins. The heat reservoir of the North Sea, and also its heat release throughout the year, is more than twice as large as that of the Baltic Sea and thus much more important for the local, regional climate of surrounding land. More than two thirds of the total heat in the Baltic Sea is stored in the Baltic Proper. The other Baltic Sea basins are of minor importance for the total heat content and release, because of their smaller volume (Gulf of Finland) and their location in higher latitudes (Gulf of Bothnia).

Only a small part of the total heat content of the water is released to the atmosphere during winter. The available heat content (Fig. 4b), i.e., the heat in the ocean which is available for release to the atmosphere, as calculated from the total heat content minus seasonal minimum heat content of the basin, shows maximum values (for the end of August) from 700 to $1600 \cdot 10^6$ J/m^2 for the different basins. Assuming a cooling period of 200 days, this corresponds for example for the North Sea to a mean heat flux of 90 W/m^2 from ocean to atmosphere. For the Baltic Sea the mean heat loss during cooling shows large differences for the sub-basins. The range is from 80 W/m^2 in the Baltic Proper to 40 W/m^2 in the Gulf of Bothnia. The differences in heat release between North Sea and Baltic Proper, which both have approximately the same latitudinal position, and thus receive a comparable heat input from shortwave radiation, can be explained by the different salinity distributions and the non-linear behaviour of the density of sea water in conjunction with sea ice, as outlined earlier. In the beginning of the cooling period in autumn, the heat fluxes in the Gulf of Bothnia or in the Baltic Proper are comparable to the fluxes in the North Sea. However, after the development of a winter thermocline and furthermore after developing of ice, the fluxes decrease very much.

3.2. *Advective heat fluxes*

The influence of advection on the heat budget can be investigated by comparing the heat content change due to advection to the total heat content change throughout the seasonal cycle. The advective heat content change is given by the cumulative advective heat transport, which is calculated by the accumulation of the net heat exchange over

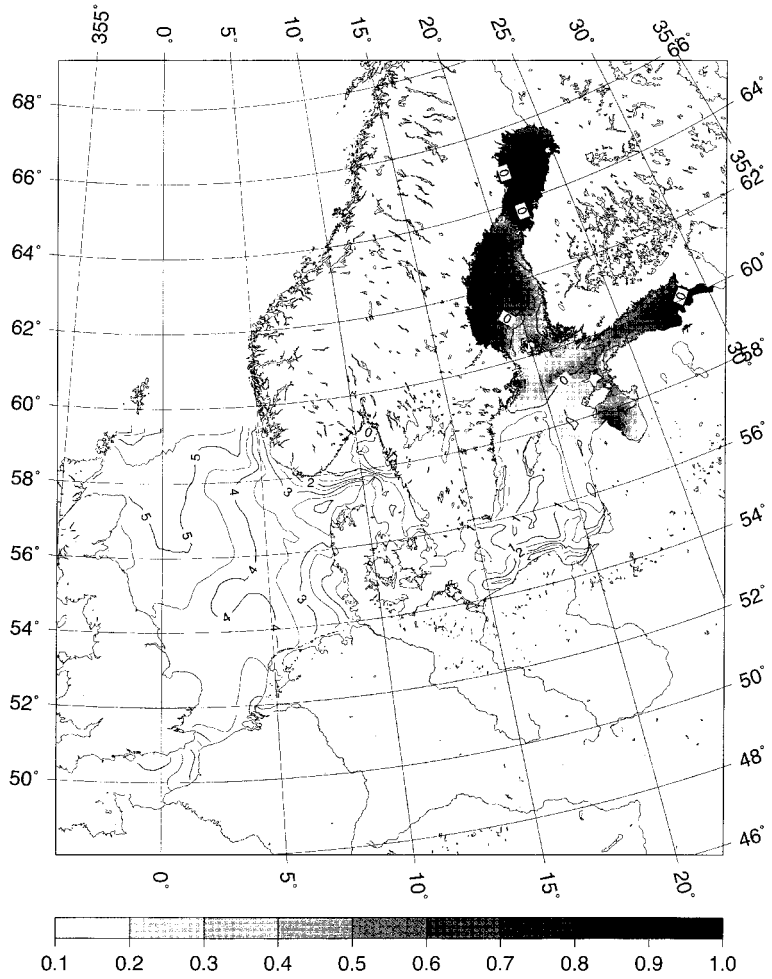

Fig. 3. Calculated sea surface temperature (°C) and ice cover for 23 March 1984 (reference case).

the boundaries of the investigated region:

$$Q_{\mathrm{cumadv}}(t) = \sum_{i=1}^{n} c_{\mathrm{p}}(\rho_{\mathrm{in}} T_{\mathrm{in}} V_{\mathrm{in}} - \rho_{\mathrm{out}} T_{\mathrm{out}} V_{\mathrm{out}})_{\mathrm{i}} + Q_{\mathrm{cumadv}}(t-1), \quad (1)$$

with t = time in days, $V_{\mathrm{in,out}}$ = volume flux across the boundaries of grid point n during 1 day, $T_{\mathrm{in,out}}$ = daily mean temperature of inflowing and outflowing water, $\rho_{\mathrm{in,out}}$ = daily mean density of inflowing and outflowing water at boundary grid point n and c_{p} = specific heat capacity.

In Fig. 4c,d the cumulative advective heat transports across the different North Sea and Baltic Sea boundaries are given.

By comparing the time series of cumulative advective heat transport into (positive) or out of (negative) the North Sea (Fig. 4c) and the Baltic Proper (positive into the Baltic Proper) (Fig. 4d) to the development of total heat content (Fig. 4a), which changes by the additional effects of advective and atmospheric heat exchange, it can be seen, that the heat exchange through the atmosphere–ocean boundary is the most substantial one. Advective processes are only in the order of 10% of the total change in heat content of the ocean throughout a year. This is the case for the exchange of heat across the North Sea boundaries as well as for the exchange through the boundaries of the Baltic Proper. This is in accordance to earlier

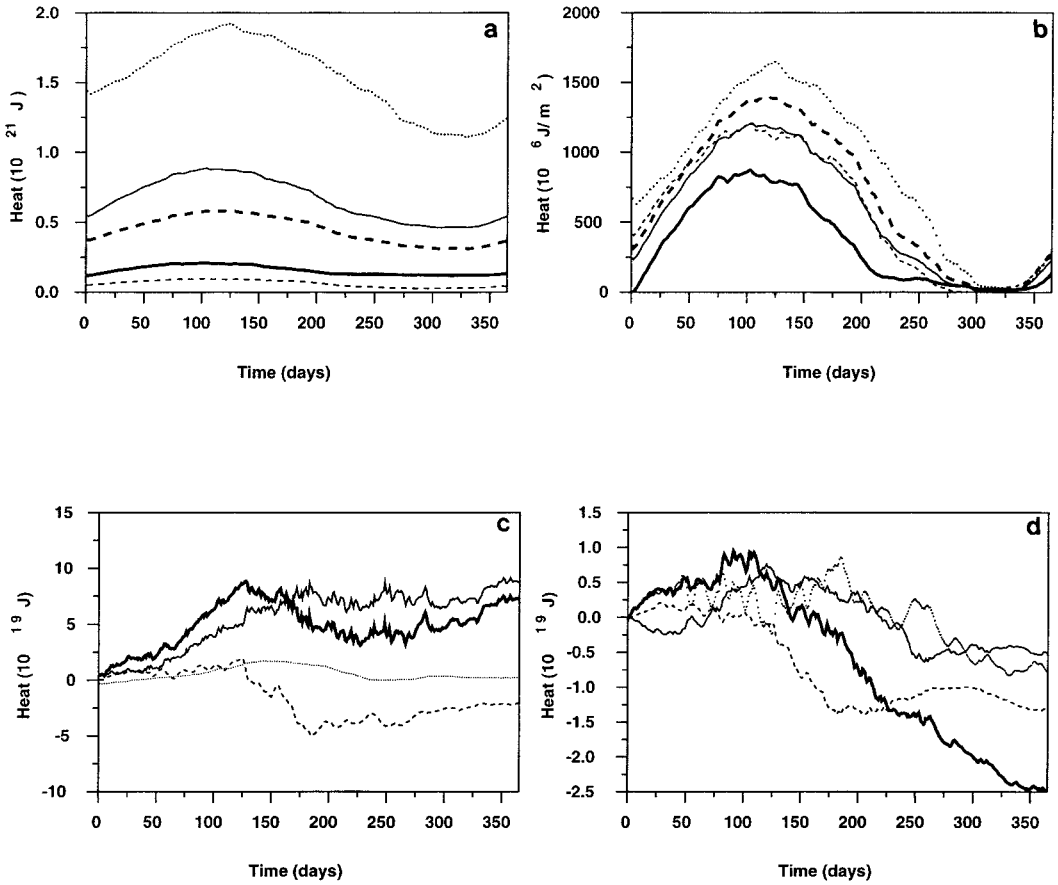

Fig. 4. (a) Temporal development of calculated total heat content in the North Sea (dotted line) and the Baltic Sea sub-basins (full line: Total Baltic; thick dashes: Baltic Proper; thick line: Gulf of Bothnia; dashed line: Gulf of Finland). The units are 10^{21} J. (b) Temporal development of heat content available for release to the atmosphere in the North Sea (dotted line) and the Baltic Sea sub-basins (full line: Total Baltic; thick dashes: Baltic Proper; dashed: Gulf of Finland; thick line: Gulf of Bothnia). The units are 10^6 J/m^2. (c,d) Temporal development of advective heat flux across the boundaries of the North Sea (c) and the Baltic Proper (d) (full line: northern boundary; dotted line: western boundary; dashed line: eastern boundary; thick line: total advective flux). The units in (c) and (d) are 10^{19} J. All time series start at 1 May 1983.

results for the North Sea, e.g. Becker (1981). However, their contribution is in the order of the interannual variability in heat content (Pohlmann, 1996b). Thus, a more detailed investigation of the fluxes across the different boundaries, and later on their sensitivity, will be carried out.

The annual value of the cumulative advective heat transport is positve for the North Sea. The North Sea gains heat by advection, this was earlier proposed by Becker (1981). Detailed investigations of the fluxes across the respective boundaries show: throughout the annual cycle, the North Sea gains heat from the Atlantic Ocean across its northern and its western boundary (English Channel). On the other hand, the North Sea exports heat to the Skagerrak. The annual cycle of the advective heat fluxes of the Baltic Proper show an overall heat loss to the Gulf of Bothnia, to the Gulf of Finland and to the Kattegat.

For the North Sea as well as for the Baltic Proper periods can be found in which the overall heat flux is turned to the opposite, i.e., a net heat export occurs in the North Sea and a net heat import occurs in the Baltic Proper. This is the

case in the spring and the early summer for the Baltic Proper. Detailed investigations show that this is caused by an import of heat from the Gulf of Finland (May/June) and from an import of heat from the Gulf of Bothnia (July/August) in addition to the temporal highly variable heat import across the western boundary of the Baltic Proper. The advective heat imports from the Gulf of Finland and the Gulf of Bothnia during this period can be explained by an outflow of warm surface water from these regions, which are partly compensated by an inflow into the Gulf of Bothnia and the Gulf of Finland in lower layers. Thus, a net heat import from these regions occurs. The import of heat across the western boundary strongly depends on the actual wind forcing as well as on the actual temperature distribution.

The heat import into the North Sea is highest during the summer and autumn months, whereby the heat export to the Skagerrak has its highest values from September to November. In combination with a stagnation of the heat import from the Atlantic, this high export of heat results in a net advective heat loss of the North Sea during this period.

4. Influence of variations in air temperature

To evaluate the influence of changes in air temperature, a sensitivity run with reduced air temperature data for the hindcast period from May 1983 to April 1984 was carried out. A constant reduction of 2°C was assumed. This is in the range of natural climate variability, as analysis of the monthly mean air temperature in the model region, taken from ECMWF re-analysis (Gibson et al., 1996), show (Fig. 5a).

4.1. Heat content

The calculations of heat content are based only on the water heat content. The heat which is stored in the ice is neglected, because the mean temperature of the ice is unknown. The ice model only gives a rough estimate of the ice surface temperature (chosen to be equal to the air temperature) and the temperature at the bottom of the ice (chosen to be equal to the freezing temperature). However, the resulting error is only small, because the volume of the ice is neglectable compared to the water volume.

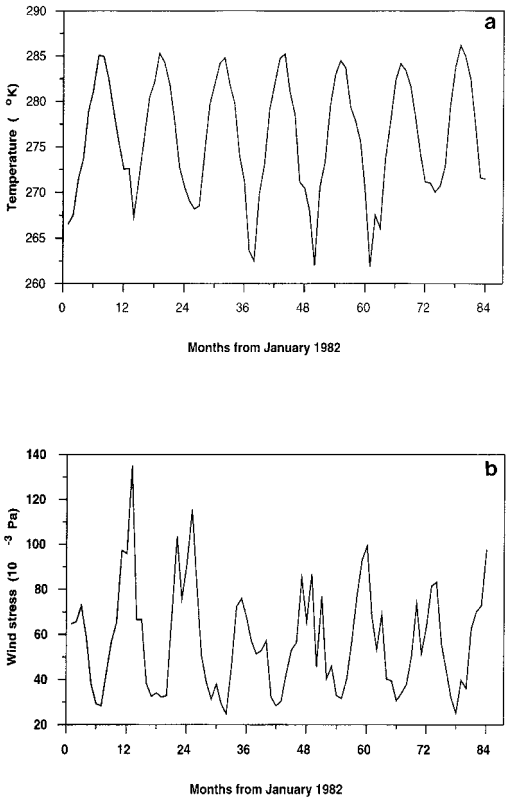

Fig. 5. (a) Monthly means of air temperature (°K) in the model region, calculated from the 2-m air temperature of the gridded ECMWF re-analysis for the period 1982–1988. (b) Monthly means of windstress in the model region, calculated from the 10 m winds of the ECMWF re-analysis for the period 1982–1988. The unit is 10^{-3} Pa.

The thermal state of the Baltic Sea and the North Sea is significantly influenced by changes in the air temperature. In Fig. 6a the difference between both cases, the reference case (i.e., normal air temperature) and the reduced air temperature case, is given for the North Sea, the Baltic Proper and the Gulf of Bothnia. A uniform decrease in heat content takes place in the three different basins. This trend is stopped in the Gulf of Bothnia around 10 November and in the Baltic Proper around 15 January when the winter thermocline, and afterwards sea ice, has developed. In the North Sea the decrease in heat content does not terminate. The increased heat flux (due to the lower air temperature) reduces the thermal energy

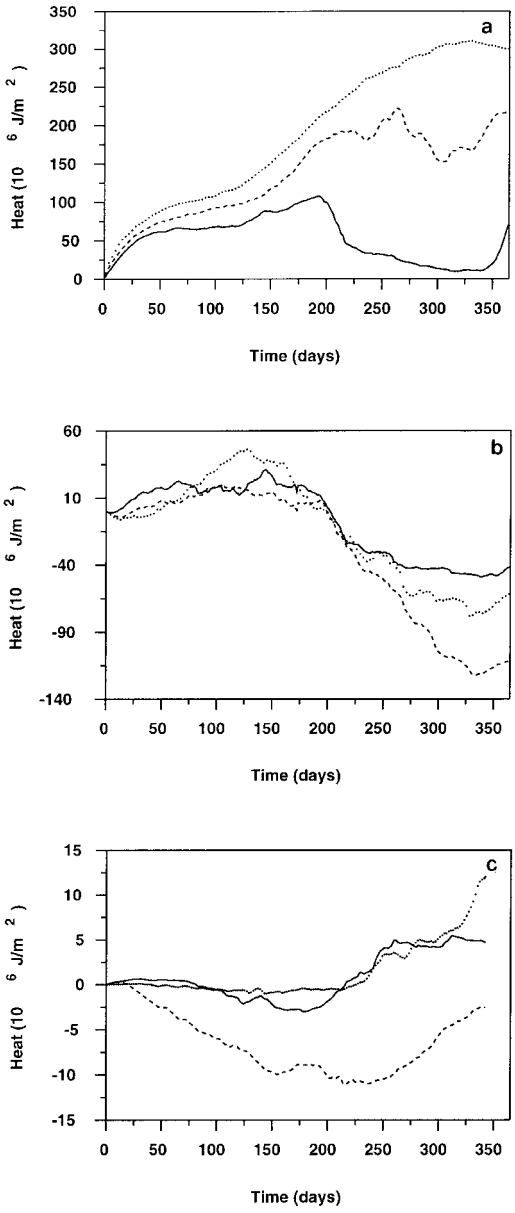

Fig. 6. (a–c) Temporal development of the difference of heat content between the reference case and reduced air temperature case (a), weaker wind case (b) and weaker fresh water runoff (c) for the Baltic Proper (dashed line), the North Sea (dotted line) and the Gulf of Bothnia (full line). The units in (a–c) are 10^6 J/m^2. All time series start at 1 May 1983.

of the North Sea further during the entire cooling period. Thus, the North Sea heat content is more sensitive to reduced air temperature than that of the Baltic Sea. At the end of the winter, the difference in heat content, as compared to the control run, is nearly twice as large in the North Sea as in the Baltic Proper.

4.2. *Advective and atmospheric heat fluxes*

In Fig. 7 the calculated changes in cumulative advective heat flux and the resulting atmospheric changes, calculated from the difference between total heat content change and the change in cumulative advective heat flux, are shown. It becomes clear that the heat content change is a measure of the atmosphere–ocean heat flux change, even if the advective heat fluxes significantly contribute to the total heat content difference between the two runs.

In the case of the North Sea as well as for the Baltic Proper, the advective heat flux differences act against the atmospheric flux differences. The Baltic Proper heat export has decreased in the case of lower air temperture. Thus, the resulting cumulative heat flux to the atmosphere is higher than the heat content change for the two runs. The resulting atmosphericflux difference after 1 year is in the order of $300 \cdot 10^6$ J/m^2, which corresponds to a constant atmospheric flux difference in the order of 15 W/m^2. For the North Sea the results are similar: The North Sea imports in the case of reduced air temperature more heat by advection. This heat is additionally released to the atmosphere, resulting in an accumulated atmospheric heat flux of $650 \cdot 10^6$ J/m^2 or a constant atmospheric heat flux change of 25 W/m^2. These results illustrate well the limitation of this simplified numerical experiment: The changes in advective heat flux are small (in the range of $50 \cdot 10^6$ J/m^2) for the region of the Baltic Proper and for the eastern and western North Sea boundaries. This is not the case for the northern boundary of the North Sea. The heat import across the northern boundary has increased up to $350 \cdot 10^6$ J/m^2. The influence of the climatological boundary conditions of temperature for the inflowing water, which have not been reduced for the sensitivity experiment, is responsible for the strong increase in advcetive heat flow across the nothern bound-

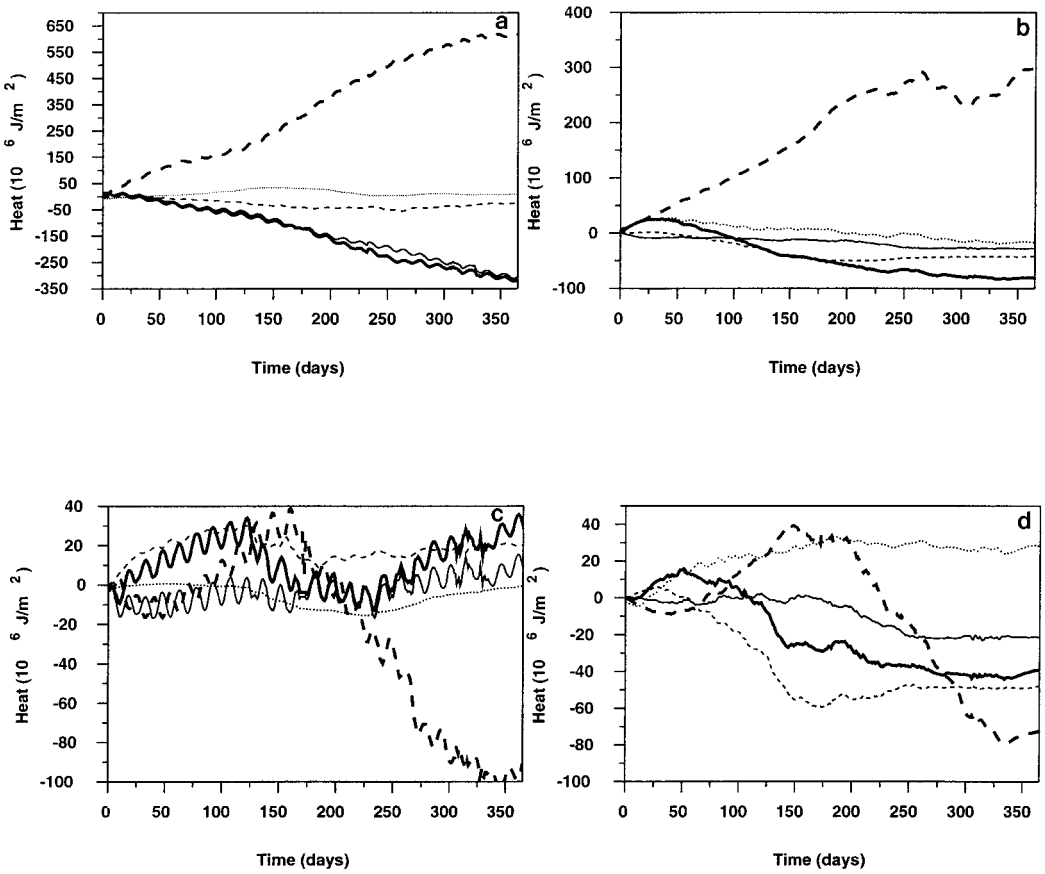

Fig. 7. (a–d) Difference between the cumulative advective and atmospheric heat fluxes. (a,b) Reference case minus reduced air temperature run for the North Sea (a) and the Baltic Proper (b). (c,d) Reference case minus reduced wind speed run for the North Sea (c) and the Baltic Proper (d). Full lines: flux across the northern boundary; dashed lines: flux across the eastern boundary; dotted lines: flux across the western boundary; thick lines: total advective fluxes; thick dashes: resulting cumulative atmospheric fluxes. The units are 10^6 J/m^2. All timeseries start at 1 May 1983.

ary in the case of reduced air temperature. This implies a resulting change in the atmospheric heat flow from the North Sea which is in the order of two times of the North Sea heat content change. The estimated range of the sensitivy of advective heat flux cannot be considered as a realistic estimate of heat flux variability due to air temperature variability, because in reality, an air temperature reduction will also have an influence on the temperatures in the North Atlantic. But, due to the fact that the temperature variability decreased from the south to the north in the North Sea (Janssen et al., 1999), the results of this sensitivty experiment will point in the right direction. Furthermore, the results illustrate well how important it is to choose apropriate boundary conditionss in long term baroclinic simulations.

4.3. Sea surface temperature and sea ice conditions

In accordance with earlier results of Omstedt and Nyberg (1996) and Haapala and Leppäranta (1997) air temperature decrease has a strong influence on sea surface temperature and thus on ice conditions. The calculated maximum ice covered area (Fig. 8a) increased from 225 000 km^2 in the reference case up to

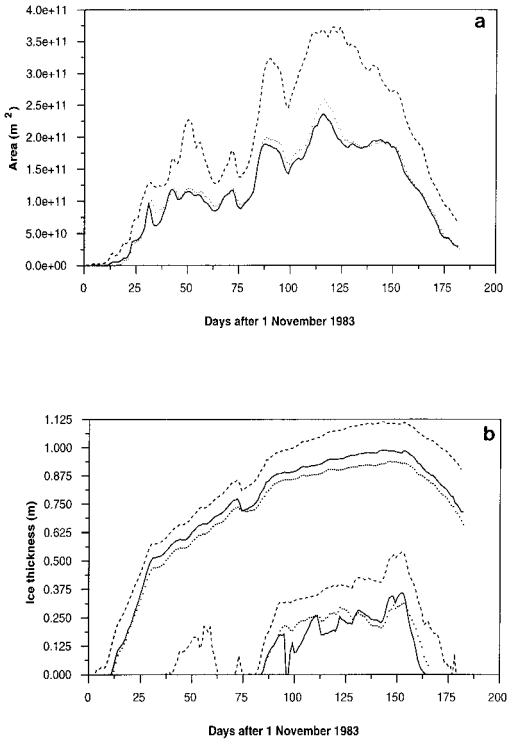

Fig. 8. (a) Sea ice development [m^2] in the Baltic Sea. (b) Calculated sea ice thickness [m]. Compared are development of the ice thickness at Kemi (upper curves) and Uto (lower three curves). The different styles of the curves indicate the three cases: the reference case (full line), the reduced air temperature case (dashed line) and the weaker wind case (dotted line). All time series start at 1 November 1983.

325 000 km^2 in the case with reduced air temperature. This is in accordance with statistical analysis of the ice area and the mean air temperature, carried out by Tinz (1996). He found a high correlation of maximum ice extend and mean air temperature in winter.

Ice thickness is also strongly influenced by air temperature changes. Near Uto the calculated ice thickness is roughly doubled by a temperature decrease of 2°C (Fig. 8b). The influence on sea surface temperature and sea ice conditions can be seen also in Fig. 9. Compared to the reference case (Fig. 3) most of the Baltic Proper is ice covered for the reduced air temperature run. In the North Sea, the differences in sea surface temperature are in the order of 2°C.

5. Influence of variations in wind speed

5.1. Heat content

For the second sensitivity run, the wind stress was reduced by one third. This is, as well as the investigated air temperature change, in the range of the natural variability in the region of North Sea and Baltic Sea, as can be seen by comparisons to the monthly mean averaged wind stress in the model region caluclated from the 10m wind in the ECMWF re-analysis (Fig. 5b). A third hindcast for the year 1983/1984 was carried out with reduced wind forcing.

The reduction in wind speed results in small differences in summer heat content in the North Sea and the Baltic (Fig. 6b). The differences are in the order of 2% of the seasonal heat release from the ocean to the atmosphere in both marginal seas. For the Baltic Proper and the Gulf of Bothnia the heat storage during summer is approximately $20 \cdot 10^6$ J/m^2 lower in the case of weaker wind forcing. For the North Sea the difference between both cases is larger, in the order of $40 \cdot 10^6$ J/m^2 at maximum.

Much more important are changes in heat content during the cooling period: a faster heat release to the atmosphere occurs for stronger winds. This is caused by increasing latent and sensible heat fluxes, which have a linear dependence on wind speed. The surplus of heat, which was received for stronger wind during summer, is completely released during the beginning of the cooling period. Later on, the sign of the differences in heat content between both cases changes and the heat content of the ocean is higher for the case of weaker wind (Fig. 6b). For the Baltic Sea, the differences in heat content between both cases are up to seven times higher during cooling than during warming. Connected are changes in the thermal stratification of the water column, as will be discussed in Subsection 5.3.

5.2. Advective and atmospheric heat fluxes

Whereby these heat content differences are caused by changing atmospheric fluxes or by changing advective heat flux needs to be investigated in more detail. In Figs. 7c,d the advective flux differences as well as the resulting cumulative atmospheric flux differences are shown for the reduced wind speed case.

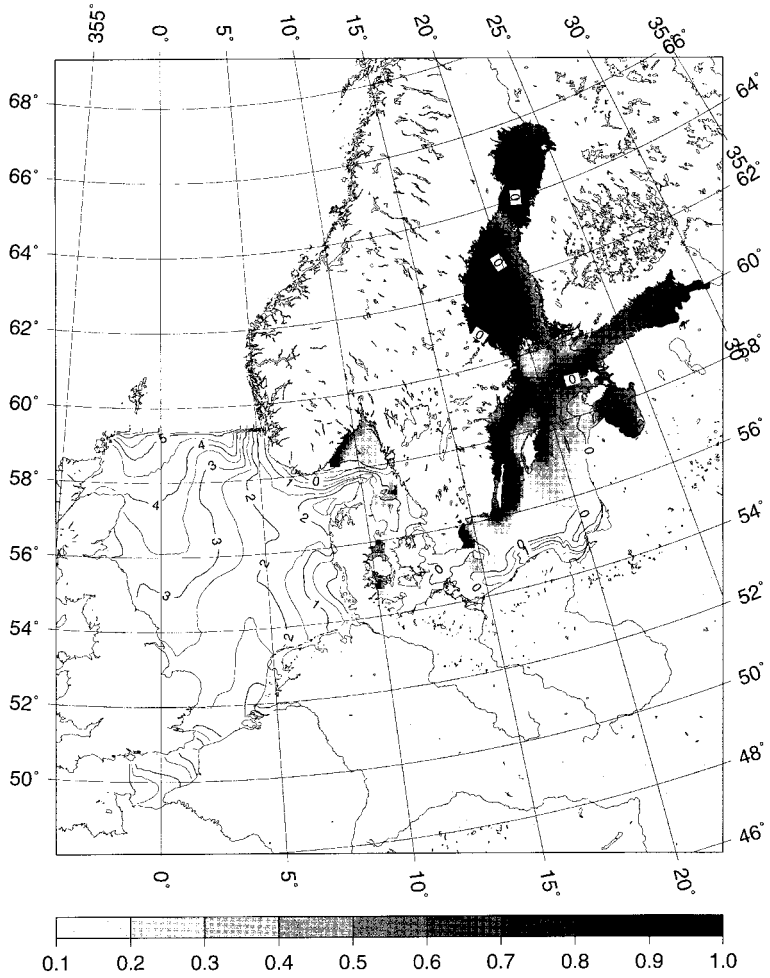

Fig. 9. Calculated sea surface temperature (°C) and ice cover for 23 March 1984 for the case of reduced air temperature.

Decreasing wind speed results for the North Sea in a decrease of the heat gain due to advection during winter and summer time as well. By comparing the advective heat content change to the atmospheric heat content change, it can be seen that a remarkable difference exists for the Baltic Proper and the North Sea. During the warming, i.e., from May to August, the changes in cumulative atmospheric heat fluxes have nearly the same values for the North Sea and for the Baltic Proper. This is not the case during the cooling period. From September to April the decrease in heat release to the atmosphere for decreasing wind is stronger for the North Sea. By comparing this to the heat content change as a result of decreasing wind speed, it can be seen that the opposite is true for the heat content change, which is stronger for the area of the Baltic Proper. This can be explained by the fact that for decreasing wind speed the heat gain of the North Sea by advection has decreased as well, thus advective and atmospheric flux changes have the opposite sign. This is not the case for the Baltic Proper. Decreasing wind speed results for the Baltic Proper in a smaller advective heat loss. Thus, advective as well as atmospheric flux differences, both contribute to the heat content increase of the Baltic Proper.

The cumulative advective flux changes at the

end of the simulation cycle amount up to a value of $100 \cdot 10^6$ J/m^2 for the North Sea and $80 \cdot 10^6$ J/m^2 for the Baltic Sea, which is equivalent to a constant atmospheric heat flux change in the order of 10 and 8 W/m^2, respectively. However, as for the reduced air temperature run, it can be seen that the heat content change is a good indicator for the atmospheric heat flux change, even if they differ in magnitute. The shape of the respective curves is similar for the North Sea as well as for the Baltic Proper.

5.3. Sea surface temperature and sea ice conditions

The sea surface temperature in the Baltic Sea, at the end of the cooling period, shows a reversed sensitivity compared to the heat content. In the case of weaker wind the surface layer is colder and thinner compared to the reference case. This is caused by the development of a shallow winter thermocline in the Baltic Sea. The thickness of this cold surface layer, and thus its temperature, depends on the strength of turbulent mixing caused by the wind stress. Comparing the ice conditions in the Baltic Sea for the two runs (Fig. 8a), it can be seen that for the weaker wind case consequently an increase in ice cover is calculated in the Baltic. The difference is up to 10% of the total calculated ice covered area. Weaker "heating" of the sea surface layer by entrainment from below, in the case of reduced wind speed, caused a colder sea surface layer and therefore earlier sea ice development and an increase in the ice covered area. However, compared to the variability induced by air temperature changes in the order of 2°C, the influence of changes in wind speed on the minimum sea surface temperature and the ice conditions is only small.

In contrast to the influence on ice cover, weaker wind leads to a thinner ice sheet, as can be seen in Fig. 8b. Decreasing wind results in weaker cooling in the already ice covered regions at the ice surface. The effect of stronger mixing in the water column due to stronger winds is not important below the ice, because momentum exchange between atmosphere and ocean is strongly reduced when ice is present. Thus, cooling at the ice surface decreases with weaker winds, but heating from below doesn't change, and therefore the sea ice grows slower, compared to the reference case. This relationship can be reversed in regions were advection has a strong influence on ice thickness, as the example for the calculated ice thickness at Uto shows (Fig. 8b).

5.4. Stratification

In Fig. 10 the calculated development of a temperature profile in the Baltic Proper is shown for the reference case. Beginning with the 1 October, every 10 days a daily mean profile was plotted. In the beginning of the cooling the temperature in the surface mixed layer decreased and thermocline deepening occurred. In a depth range from 40 to 90 m a warm intermediate layer develops between the cold surface water and the cold deep water below the halocline in the Baltic Sea. Due to the higher salinity in this warmer intermediate layer, colder surface water cannot penetrate this layer. This was earlier modelled with a 1-d convection model (Backhaus and Wehde, 1997). The development of an intermediate warmer layer during the cooling period, was observed sometimes. Two examples near the investigated position in the Baltic Proper are shown in Fig. 11. The observed temperature differences between intermediate layer and sea surface layer are up to 2°C. However, observations during the winter period are rare and thus the development of this intermediate layer during the winter 83/84 could not be illustrated by observations.

After the temperature of the local density maximum is reached, again a thermocline, which separates now colder surface water from warmer and heavier intermediate water, develops. This is well known from observations. One of the most recent publications on this winter thermocline development is from Eilola (1997).

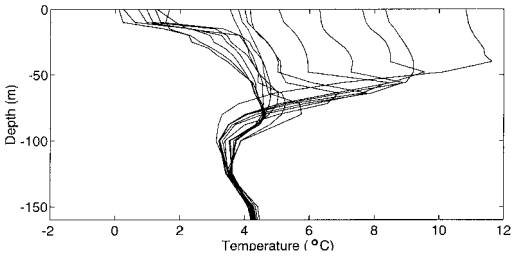

Fig. 10. Development of temperature profiles (°C) in the Baltic Proper during cooling. Profiles for every 10 days are given for the reference run. The first profile is from 1 October 1983.

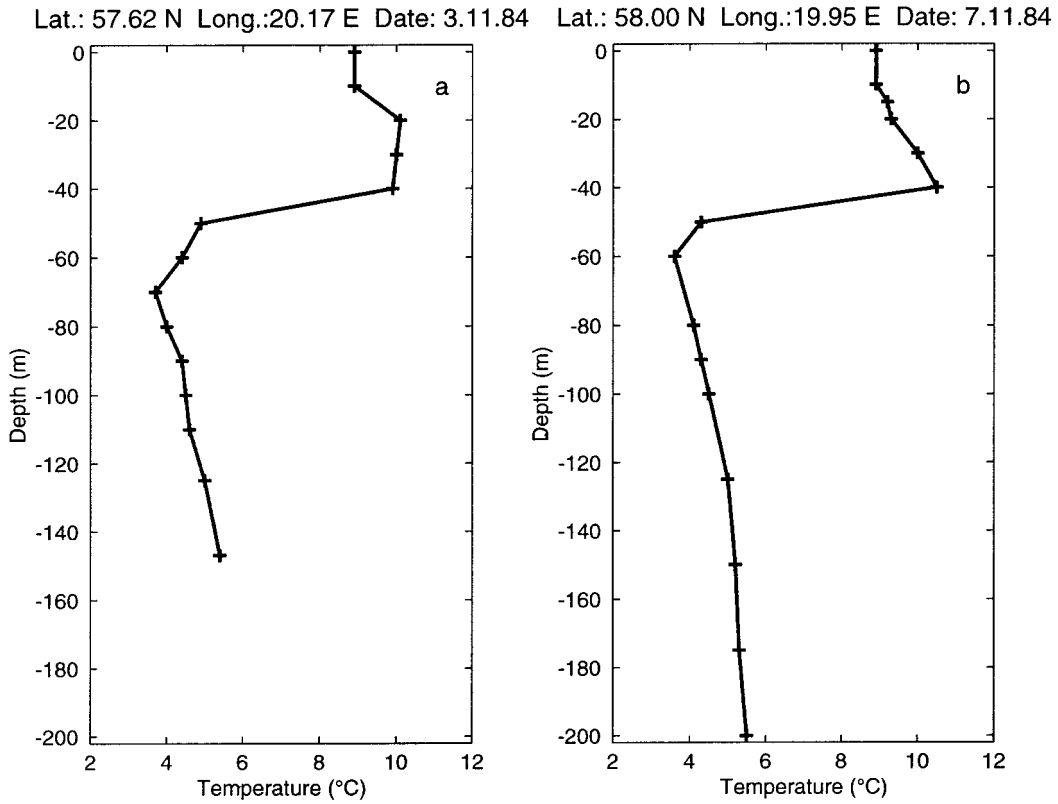

Fig. 11. Observed temperature profiles in the Baltic Proper, source: ICES data base.

The development of the vertical thermal structure is strongly influenced by changes in wind forcing and by changes in air temperature. In Fig. 12 temperature profiles (every 30 days from 1 October) for the two sensitivity runs in comparison to the reference case (dotted lines) are given. In the beginning of the cooling period, the thermocline is deeper in the reference case (i.e., normal wind) and the sea surface temperature is lower. Cooling then produces cold and heavy surface water, thermal convection starts and thermocline deepening takes place. This process is more effective for stronger winds, because the salinity of the surface mixed layer is slightly higher due to increased near surface turbulence and enhanced advection of more salty water to the Baltic Sea (Fig 13b). Thus, during cooling colder and heavier surface water is produced and thermal convection reaches deeper than in the weaker wind case.

The intermediate layer is much more pronounced and more stable in the case of weaker wind. Thus, the heating of the sea surface layer from below is reduced for weaker wind, and heat exchange with the atmosphere is hindered. At the end of the winter, a larger heat content remained in this intermediate layer in the case of weaker wind. Temperature differences between both cases of up to 2°C were calculated for this intermediate layer in the Baltic Sea. This is much more than the calculated variability of sea surface temperature, which is in the order of 0.5°C, only. A similar layer also develops in the beginning of the cooling phase in the Norwegian Coastal Current. In contrast to the Baltic, the water column below the colder surface layer is mixed much faster and the intermediate layer vanished completely with the beginning of the winter.

However, the difference between winter and

summer heat content variability is much smaller for the North Sea since haline stratification is less important for the total heat release of the North Sea. Most of its area is totally mixed by thermal convection during autumm and winter.

In early spring, when the ocean is heated again, a cold layer of winter water (CLW) develops below the sea surface and the warmer intermediate layer (Fig. 10). The temperature of this layer is estimated by the temperature of the density maximum, depending on salinity, and thus influenced by wind forcing and convection. Weaker wind leads to a warmer CLW, temperature differences up to one degree were calculated (Fig. 12b,d), and can contribute to warmer sea surface temperatures during the next spring, as earlier indicated by Eilola (1997).

6. Influence of fresh water runoff variations

The fresh water runoff was also assumed to have an important effect on heat exchange, especially in the Baltic Sea, since an influence of fresh water runoff on haline stratification was expected (Backhaus, 1996). Therefore a third sensitivity run was carried out to quantify this effect: the runoff of all fresh water sources in the North Sea and the Baltic Sea was reduced by one third which is in the order of observed climate variability of the total river runoff to the Baltic Sea (Bergström and Carlsson, 1994).

Investigation of the differences in heat content (Fig. 6c) between both fresh water cases shows: there is an effect but for the Baltic Sea the differences are one order of magnitude below the maximum wind induced change in heat content (during winter). During summer more fresh water runoff leads to a more stable stratification between turbulent surface layer and the water below. Thus, mixing into deeper parts of the ocean is slightly reduced and the heat content is smaller compared to the case of weaker runoff. During winter, the effects cancel out, an intensified stratification restrains the thermal convection.

For the North Sea the difference between both cases is of the same order as in the Baltic Sea, except for a short period in spring 1984, when a strong outflow event from the Baltic occurred. The near surface haline stratification in the Norwegian Coastal Current is influenced by the strong fresh water runoff from the Baltic and thus, the winter thermocline is intensified and heat exchange between the deeper ocean and the sea surface is reduced.

Fresh water runoff changes do only marginally influence haline stratification in the Baltic on a time scale of one seasonal cycle. The additional fresh water, which is released to the surface layer of the Baltic Sea, is, due to an increased volume of the near surface outflow and a decreased surface salinity, nearly completely released to the Belt Sea. However, results of Launiainen and Vihma (1990) show that the near bottom salinity in the Gotland Basin, and thus the intensity of the halocline, is influenced by river runoff into the Baltic with a delay of 6 years, since the salinity in the Gotland Basin depends on the salinity of inflowing North Sea water, which may depend on fresh water runoff to the North Sea and the Baltic Sea during previous years. However, the investigation of these processes on longer time scales is not possible with the simplified sensitivity experiments presented here.

7. Conclusions

Heat content changes in North Sea and Baltic Sea for a given change in air temperature or wind speed were quantified by the sensitivity experiments discussed above. It was shown that for a constant decrease in air temperature heat content and SST both are significantly reduced. However, the SST variability is not always a measure for the heat content variability in North Sea and

Fig. 12. Development of temperature (°C) profiles in the Baltic Proper for the two sensitivity cases in comparison to the reference case. (a) Profiles from 1 October 1983, every 30 days: full line, reduced air temperature case; dotted line, reference case. (b) Profiles from 1 October 1983, every 30 days: full line, reduced wind case; dotted line, reference case. (c) Profiles from 29 February 1984 and from 29 March 1984: full line, reduced air temperature case; dotted line, reference case. (d) Profiles from 29 February 1984 and from 29 March 1984: full line, reduced wind case, dotted line, reference case.

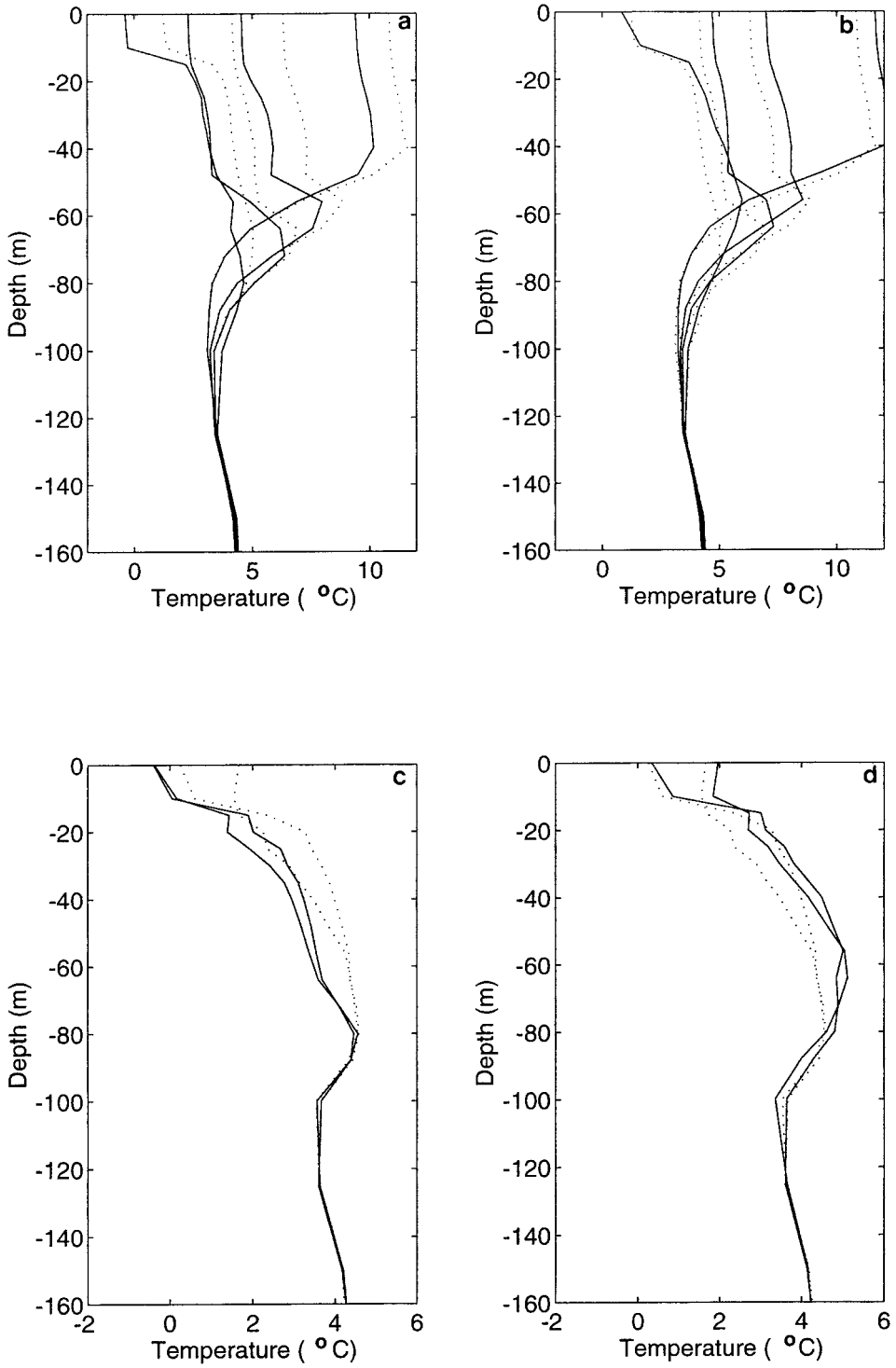
a
b
c
d
Depth (m)
Temperature (°C)
0
-20
-40
-60
-80
-100
-120
-140
-160
-2
0
2
4
5
6
10

Fig. 12.

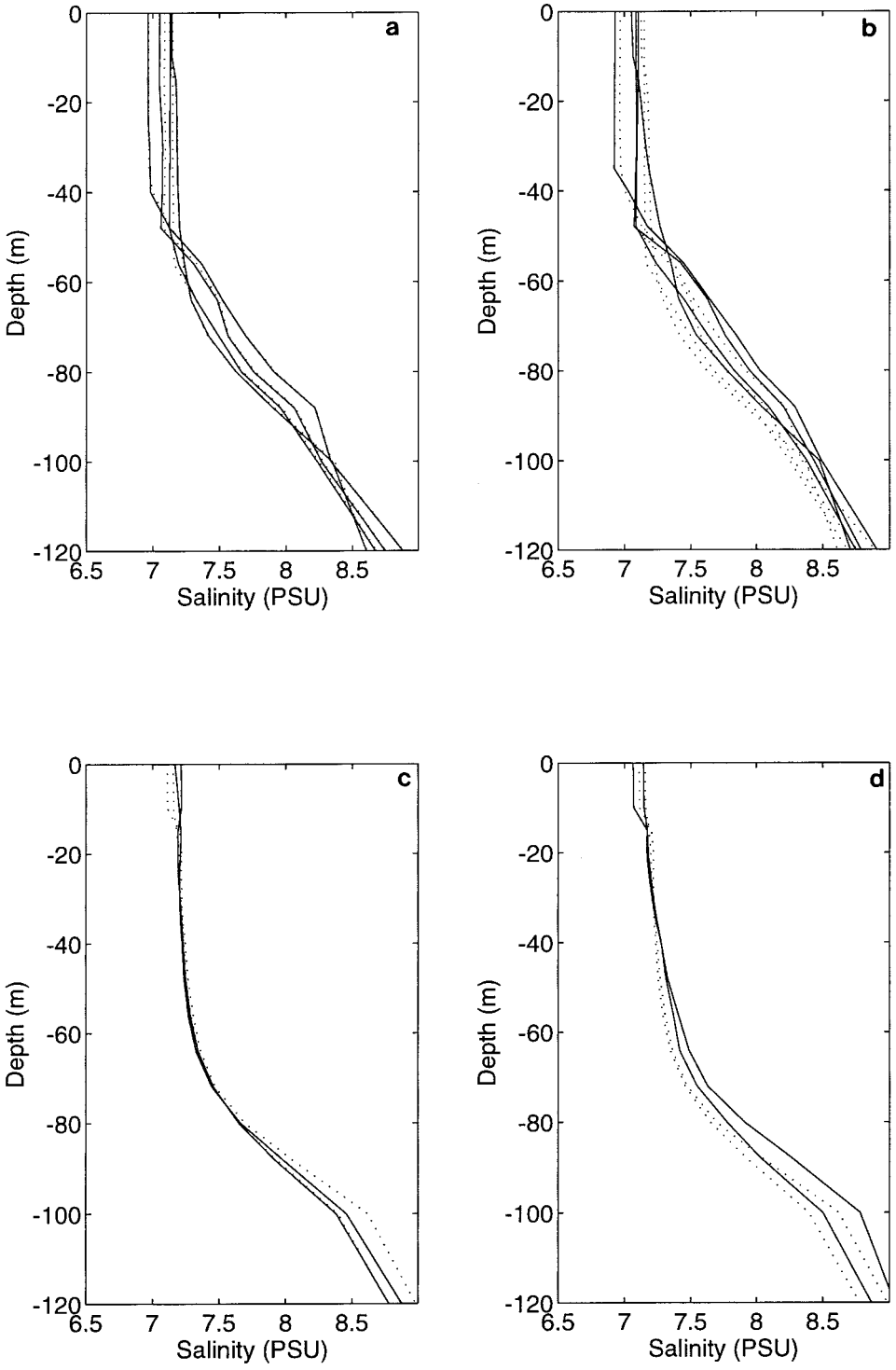

Fig. 13

Baltic Sea. In the case of reduced wind forcing, the heat content in the Baltic Sea and also in the North Sea changed without a significant change in SST during most of the time.

The type of the sensitivity experiments allows the evaluation of the direct and immediate response of the sea to the variability in atmospheric forcing only. Changing atmospheric conditions may furthermore influence the heat exchange between atmosphere and ocean on longer timescales. For example: lower temperature of the intermediate water in the Baltic Sea during the winter will decrease the SST in the following spring after the spring convection has destroyed the winter thermocline. This results in an increased heat flux from the atmosphere to the sea, and thus in an increased local cooling of the atmosphere. Atmosphere ocean interactions on longer timescales are much more complex than the direct interactions described here. Their investigation is not possible with such a simple uncoupled sensitivity experiment. However, from the results of this experiment it is clear that, especially due to the complicated reaction of the Baltic Sea and the North Sea on wind speed changes and due to the high influence of advective transports on the variability of the heat budgets, prescribed oceanic boundary conditions in local atmospheric models (for example from climatological means) or prescribed atmospheric boundary conditions in local ice–ocean models may therefore strongly limit local climate change forecasts of these models. Thus, the usage of coupled atmosphere ocean models for climate change investigations, which is already common in global climate research, appears to be necessary, also for the local scale.

8. Acknowledgements

We are thankful to all our colleagues who made it possible to carry out this study, by making available their data and parts of their models. These are S. Bergström, B. Carlsson, P. Damm, J. Haapala, M. Leppäranta, A. Omstedt, J. Paetsch and T. Pohlmann. Atmospheric boundary conditions for the model runs were kindly provided by the Deutsche Wetterdienst, Seewetteramt Hamburg. For revising the manuscript we thank H. Langenberg, J. Dellnitz and F. Janssen for preparing some figures. The study was financed by the German Ministry of Science and Technology (BMBF) under grant number 01 LK 9326/0 and 03 F0185B.

9. Appendix A

Model equations for the hydrodynamic model

The basic equations for the hydrodynamic model are the Reynolds-equations for turbulent motions, the hydrostatic approach, the equation of continuity and the equation of state. The model equations were obtained after vertical integration of the basic equations over each model layer k (note: $k = 1$ is the surface layer index, $k = K$ is the number of the bottom layer, h_k is the thickness of the model layer).

The equations for the horizontal transports in the model layer k (U_k and V_k) are based on the vertically integrated equations of motion:

$$\frac{\partial U_k}{\partial t} + \frac{\partial}{\partial x}\left(\frac{U_k U_k}{h_k}\right) + \frac{\partial}{\partial y}\left(\frac{U_k V_k}{h_k}\right) - f V_k$$

$$= -\frac{1}{\rho_k}\int_{z_k}^{z_{k-1}} \frac{\partial p}{\partial x}\,\mathrm{d}z + \frac{\partial}{\partial x} A_h \frac{\partial U_k}{\partial x} + \frac{\partial}{\partial y} A_h \frac{\partial U_k}{\partial y}$$

$$+ \left[\tau_x - wu + U\frac{\partial z}{\partial t} + uU\frac{\partial z}{\partial x} + vU\frac{\partial z}{\partial y}\right]_{z_k}^{z_{k-1}}, \quad (2)$$

Fig. 13. Development of salinity (PSU) profiles in the Baltic Proper for the two sensitivity cases in comparison to the reference case. (a) Profiles from 1 October 1983, every 30 days: full line, reduced air temperature case; dotted line, reference case. (b) Profiles from 1 October 1983, every 30 days: full line, reduced wind case, dotted line, reference case. (c) Profiles from 29 February 1984 and from 29 March 1984: full line, reduced air temperature case; dotted line, reference case. (d) Profiles from 29 February 1984 and from 29 March 1984: full line, reduced wind case; dotted line, reference case.

$$\frac{\partial V_k}{\partial t}+\frac{\partial}{\partial x}\left(\frac{U_k V_k}{h_k}\right)+\frac{\partial}{\partial y}\left(\frac{V_k V_k}{h_k}\right)+fU_k$$
$$=-\frac{1}{\rho_k}\int_{z_k}^{z_{k-1}}\frac{\partial p}{\partial y}\,\mathrm{d}z+\frac{\partial}{\partial x}A_h\frac{\partial V_k}{\partial x}+\frac{\partial}{\partial y}A_h\frac{\partial V_k}{\partial y}$$
$$+\left[\tau_y-wu+V\frac{\partial z}{\partial t}+uV\frac{\partial z}{\partial x}+vV\frac{\partial z}{\partial y}\right]_{z_k}^{z_{k-1}}, \quad (3)$$

u, v, and w are the horizontal velocities, A_h is the horizontal turbulent eddy viscosity, ρ is the density, p is the pressure and f is the Coriolis-parameter. $\tau=(\tau_x, \tau_y)$, the stress vector at the layer interfaces, the bottom and the sea surface, is defined as:

$$\tau(z)=\begin{cases}\tau_s(\zeta)/\rho_k & \text{for } z=\zeta\\ A_v\dfrac{\partial(u,v)_k}{\partial z} & \text{for } z_H<z<\zeta\\ \tau_b(z_H)/\rho_k & \text{for } z=z_H.\end{cases} \quad (4)$$

τ_s and τ_b are the surface and the bottom stress, A_v is the turbulent eddy viscosity at the layer interfaces.

Vertical integration of the equation of continuity (over one model layer), results in a diagnostic equation for the vertical velocity:

$$w_{k-1}=w_k-\frac{\partial U_k}{\partial x}-\frac{\partial V_k}{\partial y}+\left[u\frac{\partial z}{\partial x}+v\frac{\partial z}{\partial y}\right]_{z_k}^{z_{k-1}}. \quad (5)$$

Considering the kinematic boundary condition at the sea surface, a prognostic equation for the sea surface elevation ζ is obtained:

$$\frac{\partial \zeta}{\partial t}=w_1-\frac{\partial U_1}{\partial x}-\frac{\partial V_1}{\partial y}, \quad (6)$$

The pressure in the model layer k, with a thickness h_k is calculated from the hydrostatic approach:

$$p(z_k)=p(z_{k-1})+g\rho_k h_k. \quad (7)$$

The density is calculated with the non-linear equation of state after Fofonoff and Millard (1983):

$$\rho_k=\rho_k(S_k, T_k, p_k). \quad (8)$$

The model equations for temperature and salinity are derived from the principles of salt mass conservation and energy conservation. Horizontal diffusion is neglected. After vertical integration over one model layer this results in:

$$\frac{\partial S_k}{\partial t}+\frac{U_k}{h_k}\frac{\partial S_k}{\partial x}+\frac{V_k}{h_k}\frac{\partial S_k}{\partial y}$$
$$=-\frac{1}{h_k}[wS]_{z_k}^{z_{k-1}}$$
$$+\frac{1}{h_k}\left[uS\frac{\partial z}{\partial x}+vS\frac{\partial z}{\partial y}+S\frac{\partial z}{\partial t}\right]_{z_k}^{z_{k-1}}$$
$$-\frac{1}{h_k}S\left[u\frac{\partial z}{\partial x}+v\frac{\partial z}{\partial y}+\frac{\partial z}{\partial t}\right]_{z_k}^{z_{k-1}}+\frac{1}{h_k}S[w]_{z_k}^{z_{k-1}}$$
$$+\frac{1}{h_k}\left[D_v\frac{\partial S}{\partial z}\right]_{z_k}^{z_{k-1}}+\frac{\Delta S_k}{\mathrm{d}t}, \quad (9)$$

and

$$\frac{\partial T_k}{\partial t}+\frac{U_k}{h_k}\frac{\partial T_k}{\partial x}+\frac{V_k}{h_k}\frac{\partial T_k}{\partial y}$$
$$=-\frac{1}{h_k}[wT]_{z_k}^{z_{k-1}}$$
$$+\frac{1}{h_k}\left[uT\frac{\partial z}{\partial x}+vT\frac{\partial z}{\partial y}+T\frac{\partial z}{\partial t}\right]_{z_k}^{z_{k-1}}$$
$$-\frac{1}{h_k}T\left[u\frac{\partial z}{\partial x}+v\frac{\partial z}{\partial y}+\frac{\partial z}{\partial t}\right]_{z_k}^{z_{k-1}}+\frac{1}{h_k}T[w]_{z_k}^{z_{k-1}}$$
$$+\frac{1}{h_k}\left[D_v\frac{\partial T}{\partial z}\right]_{z_k}^{z_{k-1}}+\frac{\Delta T_k}{\mathrm{d}t}. \quad (10)$$

D_v is the turbulent vertical eddy diffusion. $\Delta S_k/\mathrm{d}t$ and $\Delta T_k/\mathrm{d}t$ are the salt and temperature changes due to heat and salt fluxes. River runoff and ice melting are included as sinks for the salinity and freezing is a salinity source. Salinity changes due to precipitation and evaporation are neglected for the present study. The resulting salinity change during one time step is calculated by applying mass conservation for the salt- and water mass.

10. Appendix B

Turbulence closure

The model uses a time and space dependent vertical exchange coefficient. An equation for the turbulent eddy viscosity was derived from the equation of eddy kinetic energy (Rodi, 1980). A detailed description of the concept was firstly

given by Kochergin (1987). The application of the analytical $k-\varepsilon$ approach within HAMSOM was briefly described by Pohlmann (1996a), the recent modfications were described by Schrum (1997b). The equation for the eddy viscosity at the respective layer interfaces is given by:

$$A_v = (c_L/h_{ML})^2 \sqrt{\left(\frac{\partial u}{\partial z}\right)^2 + \left(\frac{\partial v}{\partial z}\right)^2 + \frac{g}{\rho S_M}\frac{\partial \rho}{\partial z}}. \tag{11}$$

The relation between the eddy viscosity and the eddy diffusivity is given by the Schmid-number S_M (Mellor and Durbin, 1975), a function of the Richardson number

$$\mathrm{Ri} = -\frac{g}{\rho}\frac{\partial \rho}{\partial z}\Big/\left[\left(\frac{\partial u}{\partial z}\right)^2 + \left(\frac{\partial v}{\partial z}\right)^2\right]:$$

$$S_M = A_v/D_v, \tag{12}$$

with

$$S_M = \mathrm{Ri}/(0.725(\mathrm{Ri} + 0.186 - \sqrt{\mathrm{Ri}^2 - 0.316\mathrm{Ri} + 0.0346})). \tag{13}$$

The coefficient c_L was estimated by Kochergin for a large-scale, stationary case. He obtained the result $c_L = 0.05$. This value was confirmed by Pohlmann (1996a) for a general circulation North Sea model and is used in general in the HAMSOM. h_{ML} is the actual mixed layer thickness. h_{ML} is calculated in dependence of the Richardson number (Pohlmann, 1996a; Schrum, 1997b).

11. Appendix C

Model equations of the dynamic sea ice model

The development of ice is described by three parameters: the ice compactness A_i (the fraction of the grid cell which is covered by ice), the level ice thickness h_l and the thickness of the ridged ice h_r. In conjunction with the ice compactness it is possible to have ice and open water in the same grid cell. This leads to two different ice thicknesses: the average ice thickness H and the effective thickness h_i. Both are linked via the ice compactness A_i:

$$H = h_i A_i, \tag{14}$$

with

$$h_i = h_l + h_r. \tag{15}$$

After assuming a steady state and neglecting the influence of the sea level elevation on the ice drift, the model equations for the drift velocity of the ice $\boldsymbol{V}_i = (u_i, v_i)$ are given by:

$$-\rho_i(h_l + h_r) f v_i = \tau_{a(x)} + \tau_{w(x)} + \nabla\Sigma, \tag{16}$$

$$\rho_i(h_l + h_r) f u_i = \tau_{a(y)} + \tau_{w(y)} + \nabla\Sigma. \tag{17}$$

τ_a and τ_w are the stress vectors at the ice–atmosphere and the ice–water interfaces. The internal ice stress Σ are calculated by applying the nonlinear viscous plastic constitutive law after Hibler (1979).

Equations for the dynamical change of the ice thickness and the ice concentration are obtained by applying the conservation equations for the ice mass on the different ice levels (open water $(1 - A_i)$, level ice and ridging ice).

$$\frac{\partial(A_i, h_l, h_r)}{\partial t} = -\boldsymbol{V}_i \nabla (A_i, h_l, h_r) + (\Phi_A, \Phi_L, \Phi_R). \tag{18}$$

The mechanical deformation functions (Φ_A, Φ_L, Φ_R) describe open water changes, rafting and ridging. They must satisfy the following equation:

$$h_i \Phi_A + A_i(\Phi_L + \Phi_R) = -h_i A_i \nabla \boldsymbol{V}_i. \tag{19}$$

The sea ice model is a "tree-level-scheme": Following Leppäranta (1981) (see also Omstedt et al., 1994), three cases are distinguished:

1. If the ice concentration is less than one or if there is a divergence in the ice pack, convergences or divergences in the ice flow field change only the ice concentration:

$$\Phi_L = \Phi_R = 0, \tag{20}$$

$$\Phi_A = -A_i \nabla \boldsymbol{V}_i. \tag{21}$$

2. If the ice concentration is equal to one and the ice thickness is below the critical thickness (0.1 m), converging ice drift changes the level ice thickness, i.e., rafting occurs:

$$\Phi_A = \Phi_R = 0, \tag{22}$$

$$\Phi_L = -h_i \nabla \boldsymbol{V}_i. \tag{23}$$

3. If the ice concentration is equal to one, the ice thickness is above the critical thickness and the ice drift converges, ridging occurs:

$$\Phi_A = \Phi_L = 0, \tag{24}$$

$$\Phi_R = -h_i \nabla \boldsymbol{V}_i. \tag{25}$$

12. Appendix D

Thermodynamics and model coupling

The ice model and the hydrodynamic model are coupled by the fluxes of heat, salt and momentum. The heat (Q_s) and momentum fluxes (i.e., the sea surface stress) across the sea surface are a function of the ice cover:

$$Q_s = (1 - A_i)Q_w + A_i Q_i, \tag{26}$$

$$\tau_s = (1 - A_i)\tau_a - A_i \tau_w. \tag{27}$$

The heat flux between the open water and the atmosphere (Q_w) is a function of wind velocity, air temperature, specific humidity and cloud cover. It is calculated from bulk formulae for latent (Q_l) and sensible heat flux (Q_s), long-wave radiation and global radiation:

$$Q_w = Q_s + Q_l - Q_{rl} + Q_{rs}. \tag{28}$$

The turbulent heat fluxes (Q_s and Q_l) and the long-wave thermal radiation (Q_{rl}) are carried into the first model layer whereby the heat input due to short-wave radiation (Q_{rs}) is distributed over the first 50 m of the water column.

The decay of the intensity of the global radiation is approximated by a bi-modal decay law (Paulsen und Simpson, 1977):

$$I(z) = Q_{RS}(C^* \, e^{\lambda_1 (z-D)} + (1 - C^*) \, e^{\lambda_2 (z-D)}). \tag{29}$$

The extinct coefficients λ_1 and λ_2 describe the decay of the intensity of solar insulation due to absorbation and scattering due to suspended and dissolved material. They are a function of the wavelength. C^* is the contribution of the short-wave radiation which can be approximated by the extinct coefficient λ_1.

Following condition needs to be hold to fulfil energy conservation for the bi-modal decay law:

$$C^*/\lambda_1 + (1 - C^*)/\lambda_2 = 1. \tag{30}$$

The heating and cooling of the water is calculated by applying heat budget equations for the respective water levels. The thermodynamic temperature change of this layer during one time step, caused by the heat flux Q_k into this layer, is estimated by:

$$\Delta T_k = \mathrm{d}t \; Q_k/(c_p^w \rho_k h_k). \tag{31}$$

c_p^w, the specific heat capacity of sea water, is a function of temperature and salinity, after Fofonoff (1962).

The minimum water temperature is the freezing temperature T_f, a function of salinity (Millero, 1978). If the freezing temperature is reached, supercooling results in sea ice development. The newly formed ice f_0 is determined by the rate of supercooling (Q_{sc}). In this case, the initial ice thickness development f_0 is given by:

$$f_0 = \frac{\partial h_l}{\partial t} = -\frac{Q_{sc}}{\lambda_i \rho_i}, \tag{32}$$

whereby λ_i is the latent heat of ice.

If there is already ice on the water, an additional heat balance equation for the ice is considered:

$$f_h = \left(\frac{\partial h_l}{\partial t}\right)_b + \left(\frac{\partial h_l}{\partial t}\right)_t. \tag{33}$$

At the lower ice boundary, at the ice–water interface, freezing or melting of the ice is possible. Following Harms (1994), two heat fluxes are considered: the ice–ocean heat flux Q_i and the conductive heat flux through the ice Q_c.

$$\rho_i \lambda_i \left(\frac{\partial h}{\partial t}\right)_b = Q_i + Q_c. \tag{34}$$

At the ice surface, only melting, as a function of the heat flux at the ice surface Q^i is possible. In this case, the heat balance equation is given by:

$$\rho_i \lambda_i \left(\frac{\partial h}{\partial t}\right)_t = Q^i. \tag{35}$$

The equation for the ice mass change is modified by considering the thermodynamic changes of the ice, i.e., freezing and melting:

$$\frac{\mathrm{d}H}{\mathrm{d}t} = A_i f_h + (1 - A_i) f_0. \tag{36}$$

The volume change at the ice ocean interface due to freezing or melting is given by:

$$\rho_w \frac{\partial h_k}{\partial t} = \rho_i (A_i f_h + (1 - A_i) f_0). \tag{37}$$

The salt flux due to freezing and melting is calculated by applying mass conservation on the salt- and the water mass, assuming a salinity of the ice of 20% of the respective water salinity.

The thermodynamic variation of the ice compactness is calculated with a freezing or a melting

equation introduced by Hibler (1979):

$$\left(\frac{\partial A_i}{\partial t}\right)_{\mathrm{T}} = \begin{cases} f_0 \dfrac{(1-A_i)}{h_0} \Rightarrow f_0 > 0 & \text{(freezing)} \\ f_{\mathrm{h}} \dfrac{A_i}{2h} \Rightarrow f_{\mathrm{h}} < 0 & \text{(melting)} \end{cases} \tag{38}$$

with $h_0 = 0.5$ m.

13. Appendix E

Bulk formulae

The sea surface wind stress τ_{a} is a function of wind velocity $\boldsymbol{V}_{\mathrm{a}}$. The wind stress is calculated with a bulk formula given by Luthardt (1987):

$$\tau_{\mathrm{a}}(\zeta) = c_{\mathrm{da}} \boldsymbol{V}_{\mathrm{a}} |\boldsymbol{V}_{\mathrm{a}}|, \tag{39}$$

with

$$c_{\mathrm{da}} = \rho_{\mathrm{a}}(1.18 + 0.016|V_{\mathrm{a}}|)10^{-3}. \tag{40}$$

The stress at the upper ice boundary is equal to the sea surface wind stress. The stress at the ice–ocean interface (τ_{w}) is a function of the difference between water ($\boldsymbol{V}_{\mathrm{w}}$) and ice velocity ($\boldsymbol{V}_i$). It is given by:

$$\tau_{\mathrm{w}} = c_{\mathrm{dw}}|(\boldsymbol{V}_{\mathrm{w}} - \boldsymbol{V}_i)|(\boldsymbol{V}_{\mathrm{w}} - \boldsymbol{V}_i), \tag{41}$$

with

$$c_{\mathrm{dw}} = \rho_{\mathrm{w}} 0.0055.$$

The bulk formulae for sensible (Q_{s}) and latent (Q_{l}) heat flux between open water and the atmosphere are functions of the temperature- and humidity differences between the sea surface (indicated by the subscript *w*) and the atmosphere at a height of 10 m (indicated by the subscript *a*):

$$Q_{\mathrm{s}} = \rho_{\mathrm{a}} c_{\mathrm{p}}^{\mathrm{a}} |V_{\mathrm{a}}| C_{\mathrm{H}}(T_{\mathrm{a}} - T_{\mathrm{w}}), \tag{43}$$

$$Q_{\mathrm{l}} = \lambda_{\mathrm{w}} \rho_{\mathrm{a}} |V_{\mathrm{a}}| C_{\mathrm{L}}(q_{\mathrm{a}} - q_{\mathrm{w}}). \tag{44}$$

C_{H} and C_{L} are exchange coefficients for sensible and latent heat flux, depending on atmospheric stratification and wind speed; estimates are chosen following Kondo (1975). λ_{w} is the latent heat of water.

The long-wave radiation (Q_{rl}) is estimated after the radiation law of Boltzmann by the following bulk formula:

$$Q_{\mathrm{rl}} = \varepsilon_{\mathrm{w}} c_{\mathrm{Boltz}} T_{\mathrm{w}}^4 - \varepsilon_{\mathrm{a}} c_{\mathrm{Boltz}} T_{\mathrm{a}}^4. \tag{45}$$

c_{Boltz} is the Boltzman constant, ε_{w} and ε_{a} are the emissive power for the ocean and for the atmosphere. ε_{w} is assumed to be equal 0.97. The emissive power of the atmosphere depends on cloudiness c_n, calculated with a bulk formula given by Maykut (1986):

$$\varepsilon_{\mathrm{a}} = 0.7855(1 + 0.2232 c_n^{2.75}). \tag{46}$$

The global radiation (Q_{rs}), the total amount of short-wave radiation and diffusive sky radiation, is calculated after the OKTA model of Dobson and Smith (1988):

$$Q_{\mathrm{rs}} = S \sin(s_n)(A^* + B^* \sin(s_n))(1 - R_{\mathrm{A}}). \tag{47}$$

S is the solar constant for the eighties (after Lee et al. (1988) equal to 1365). s_n is the sun altitude and R_{A} is the water albedo and calculated as a function of sun altitude (Becker, 1981). A^* and B^* are coefficients depending on cloud cover.

The heat flux between ice and water is given by (Harms, 1994):

$$Q_i = \rho_{\mathrm{w}} c_{\mathrm{p}}^{\mathrm{w}} A_{\mathrm{v}} \frac{(T_i^{\mathrm{l}} - T_{\mathrm{w}})}{\mathrm{d}z_1}, \tag{48}$$

and the conductive heat flux through the ice is given by (Maykut, 1986):

$$Q_{\mathrm{c}} = \frac{\kappa}{h}(T_i^{\mathrm{l}} - T_i^{\mathrm{u}}). \tag{49}$$

For the heat conductivity of ice (κ) a value of $\kappa = 2.1$ is used. T_i^{l} and T_i^{u} are the temperatures of the ice at the upper and lower boundary. The temperature of the lower ice boundary (T_i^{l}) is equal to the freezing temperature of the water T_{f}. Following Omstedt et al. (1995), the ice surface temperature (T_i^{u}) is assumed to be equal to the air temperature.

The respective contributions to the heat flux at the upper ice boundary (Q^i) are the short-wave radiation to the ice Q_{rs}^i, the net long-wave radiation (Q_{rl}^i), the turbulent fluxes between the ice and the atmosphere and the conductive heat flux through the ice.

$$Q^i = Q_{\mathrm{s}}^i + Q_{\mathrm{l}}^{\mathrm{i}} - Q_{\mathrm{rl}}^i + Q_{\mathrm{rs}}^i - Q_{\mathrm{c}}. \tag{50}$$

The global radiation for ice is estimated from eq. (47), using an albedo of 0.65 for the ice surface. The effective long-wave radiation of the ice, is calculated after the radiation law of Boltzmann following eqs. (45) and (46), and the sensible heat

flux between ice and water is calculated after eq. (43), by using ice surface temperatures instead of water temperatures. The latent heat flux is calculated after eq. (44), considering the sum of latent heat of ice and latent heat of water instead of just latent heat of water. A ratio of 1.2/0.55 is assumed between the transfer coefficient C_L for water and the respective coefficient for the ice.

REFERENCES

BALTEX, *Baltic Sea Experiment. 1995. Initial Implementation Plan.* International BALTEX Secretariat, 2, 84 pp.

Backhaus, J. O. 1985. A three-dimensional model for the simulation of shelf sea dynamics. *Deutsche Hydrographische Zeitschrift* **38**, 165–187.

Backhaus, J. O. 1996. Climate sensitivity of European coastal seas. *J. Marine Systems* **7**, 361–382.

Backhaus, J. O. and Hainbucher, D. 1987. A finite difference general circulation model for shelf seas and its application to low frequency variability on the North European Shelf. Three-dimensional models of marine and estuarine dynamics (eds. Nihoul, J. C. J. and Jamart, B. M.). *Elsevier Oceanography Series* **45**, 221–244.

Backhaus, J. O. and Wehde, H. 1997. Convection in the Baltic Sea. A numerical process study. In: *Sensitivity of North Sea, Baltic Sea and Black Sea to anthropogenic and climatic changes* (eds. Özsoy, E. and Mikaelyna, A.). Nato ASI Ser., Kluwer Academic Publishers, pp. 295–309.

Becker, G. A. 1981. Beiträge zur Hydrographie und Wärmebilanz der Nordsee. *Deutsche Hydrographische Zeitschrift* **34**, 167–262.

Bergström, S. and Carlsson, B. 1994. River runoff to the Baltic Sea: 1950–1990. *Ambio* **23**, 280–287.

Cubasch, U., Hasselmann, K., Höck, H., Maier-Reimer, E., Mikolajewicz, U., Santer, D. and Sausen, R. 1992. Time-dependent greenhouse warming computations with a coupled ocean–atmosphere model. *Clim. Dyn.* **8**, 55–69.

Cubasch, U., Hegerl, G., Hellbach, A., Höck, H., Mikolajewicz, U., Santer, D. and Voss, R. 1995. A climate change simulation starting 1935. *Clim. Dyn.* **11**, 71–84.

Daji, H. 1995. Modelling studies of barotropic and baroclinic dynamics in the Bohai Sea. Berichte aus dem Zentrum für Meeres- und Klimaforschung der Universität Hamburg, Germany. Reihe B. *Ozeanographie* **17**, 126 pp.

Damm, P. 1997. Die saisonale Salzgehalts- und Frischwasserverteilung in der Nordsee und ihre Bilanzierung. Berichte aus dem Zentrum für Meeres- und Klimaforschung der Universität Hamburg, Germany. Reihe B. *Ozeanographie* **28**, 259 pp.

Dobson, F. W. and Smith, S. D. 1988. Bulk models of solar radiation at sea. *Q. J. R. Meteorol. Soc.* **114**, 165–182.

Eilola, K. 1997. Development of a spring thermocline at temperatures below the temperature of maximum density with application to the Baltic Sea, *Journal of Geophysical Research* **102**, no. C4, 8657–8662.

Fofonoff, N. P. 1962. Physical properties of sea-water. *The Sea* (ed. Hill, M. N.), ch. 1, pp. 3–30.

Fofonoff, N. P. and Millard Jr, R. C. 1983. *Algorithms for computation of fundamental properties of sea water.* UNESCO Technical Papers in Marine Science, 44.

Gibson, R., Kallberg, P. and Uppala, S. 1996. The ECMWF Re-Analysis (ERA) project. *ECMWF Newsletter* **73**, 7–17.

Haapala, J., Alenius, P., Dubra, J., Klyachkin, S. V., Kouts, T., Leppäranta, M., Omstedt, A., Pakstys, L., Schmelzer, N., Schrum, C., Seinä, A., Strübing, K., Sztobryn, M. and Zaharchenko, E. 1996. Ice data bank for Baltic Sea climate studies. *Report Series in Geophysics* (University of Helsinki) **35**, 45 pp.

Haapala, J., Leppäranta, M. and Omstedt, A. 1993. Data programme for Baltic Sea ice climate modelling. Proc. 1st Workshop on the Baltic Sea Ice Climate, Tvärminne, Finland, 24–26 August 1993. *Report Series in Geophysics* (University of Helsinki) **27**, 95–107.

Haapala, J. and Leppäranta, M. 1997. The Baltic Sea Ice season in changing climate. *Boreal. Env. Res.* **2**, 1–16.

Harms, I. 1994. *Numerische Modellstudie zur winterlichen Wassermassenformation in der Barentssee.* Berichte aus dem Zentrum für Meeres- und Klimaforschung der Universität Hamburg, Germany, Reihe B, 7, 97 pp.

HELCOM. 1986. Water balance of the Baltic Sea. A regional Cooperation Project of the Baltic Sea States. International Summary Report. *Baltic Sea Environment Proceedings* **16**, 174 S.

Heyen, H., Zorita, E. and von Storch, H. 1996. Statistical downscaling of monthly mean North Atlantic air-pressure to sea-level anomalies in the Baltic Sea. *Tellus* **48A**, 312–323.

Hibler, W. D. 1979. A dynamic thermodynamic sea ice model. *J. Phys. Oceanogr.* **9**, 815–846.

Janssen, F., Schrum, C. and Backhaus, J. 1999. A climatological dataset of temperature and salinity for the North Sea and the Baltic Sea. *Deutsche Hydrographische Zeitschrift*, in press.

Johns, T. C., Carnell, R. E., Crossley, J. F., Gregory, J. M., Mitchell, J. F. B., Senior, C. A., Tett, S. F. B. and Wood, R. A. 1997. The second Hadley Centre coupled ocean–atmosphere GCM: model description, spinup, validation. *Clim. Dyn.* **13**, 103–134.

Kochergin, V. P. 1987. Three-dimensinal prognostic models. In: *Three-dimensional coastal ocean models* (ed.

Heaps, N. S.). *Coastal and Estuarine Sciences*, **4**, 201–208.

Kondo, J. 1975. Air–sea bulk transfer coefficients in diabatic conditions. *Boundary-layer Meteorology* **9**, 91–112.

Launiainen, J. and Vihma, T. 1990. Meteorological, ice and water exchange conditions. Second periodic assessment of the state of the marine environment of the Baltic Sea, 1984–1988; Background document. *Baltic Sea Environment Proc.* **35B**, 22–33.

Lee, R. B. et al. 1988. Earth radiation budget satellite extra-terrestrial solar constant measurements: 1986–1987 increasing trend. *Adv. Space Res.* **8** (7), 11–13.

Leppärranta, M. 1981. An ice drift model for the Baltic Sea. *Tellus* **33**, 583–596.

Luthardt, H. 1987. Analyse der wassernahen Druck- und Windfelder über der Nordsee aus Routinebeobachtungen. *Hamburger Geophysikalische Einzelschriften.* **83**.

Matthäus, W. 1995. Natural variability and human impacts reflected in long-term changes in the Baltic Deep Water Conditions. A Brief Review. *Deutsche Hydrographische Zeitschrift* **47**, 47–65.

Maykut, G. A. 1986. The surface heat and mass balance. *The geophysics of sea ice.* Plenum Press, New York.

Mellor, G. L. and Durbin, P. A. 1975. The structure and dynamics of the ocean surface mixed layer. *Journal of Physical Oceanography* **5**, 718–728.

Millero, F. J. 1978. Freezing point of seawater. In: *Eighth Report of the Joint Panel on Oceanographic tables and standards.* Unesco Techn. Pap. Mar. Sci., No. 28, Annex 6.

Omstedt, A. and Nyberg, L. 1996. Response of Baltic Sea ice to seasonal interannual forcing and climate change. *Tellus* **48A**, 644–662.

Omstedt, A., Nyberg, L. and Leppäranta, M. 1994. A coupled ice–ocean model supporting winter navigation in the Baltic Sea. Part 1: Ice dynamics and water levels. *SMHI Reports* **17**, 17 pp.

Omstedt, A. and Nyberg, L. 1995. A coupled ice–ocean model supporting winter navigation in the Baltic Sea. Part 2: Thermodynamics and meteorological coupling. *SMHI Reports* **21**, 30 pp.

Omstedt, A., Meueller, L. and Nyberg, L. 1997. Interannual, seasonal and regional variations of precipitation and evaporation over the Baltic Sea. *Ambio*, in press.

Paulson, A. and Simpson, J. 1977. Irradiance measurements in the upper ocean. *Journal of Physical Oceanography* **7**, 952–956.

Pohlmann, T. 1996a. Predicting the thermocline in a circulation model of the North Sea. Part I: Model description, calibration and verification. *Cont. Shelf Res.* **16**, 131–146.

Pohlmann, T. 1996b. Simulating the heat storage in the North Sea with a three-dimensional circulation model. *Cont. Shelf Res.* **16**, 195–213.

Rodi, W. 1980. *Turbulence models and their application in hydraulics. A state of the art review.* International Association for Hydraulics, Delft.

Roeckner, E., Arpe, K., Bengsson, L., Brinkop, S. Duemenil, L., Esch, M. Kirk, E., Lunkheit, F., Ponater, M., Rockel, B., Sausen, R., Schlese, U., Schubert, S. and Windelband, M. 1992. *Simulation of the present day climate with the ECHAM model: impact of model physics and resolution.* Report 93, Max-Planck Institut für Meteorologie, Hamburg, Germany.

Schrum, C. 1997a. A coupled ice–ocean model for the North Sea and the Baltic Sea. Sensitivity of North Sea, Baltic Sea and Black Sea to anthropogenic and climatic changes. In: *Sensitivity of North Sea, Baltic Sea and Black Sea to anthropogenic and climatic changes* (eds. Özsoy, E. and Mikaelyna, A.). Nato ASI Ser., Kluwer Academic Publishers, pp. 311–325.

Schrum, C. 1997b. Thermocline development and instabilities at tidal mixing fronts. Results of an eddy resolving model for the German Bight. *Cont. Shelf Res.* **17**, 689–716.

Stigebrand, A. 1983. A model for the exchange of water and salt between the Baltic and the Skagerrak. *J. Phys., Oceanogr.* **13**, 411–427.

Von Storch, H. 1994. *Inconsistencies at the interface of climate impact studies and global climate research.* Report No. 122, Max-Planck-Institut für Meteorologie, Hamburg, Germany.

Stronach, J. A., Backhaus, J. O. and Murty, T. S. 1993. An update on the numerical simulation of oceanographic processes in the waters between Vancouver Island and the Mainland: the GF8 model. *Oceanogr. Mar. Biol. Annu. Rev.* **31** (UCL Press), 1–87.

Tinz, B. 1996. On the relation between annual maximum extent of ice cover in the Baltic Sea and sea level pressure as well as air temperature field. *Geophysica* **32**, 319–341.